analytical chemistry

Effect of Redox Mediators on Corrosion Behavior and Scanning Electrochemical Microscopy Response

Emmanuel Mena-Morcillo, Ali Ebrahimzadeh Pilehrood, Reza Moshrefi, Ghazal Shafiee,
Peter George Keech, Mehran Behazin, and Samantha Michelle Gateman*

Cite This: *Anal. Chem.* 2024, 96, 9122−9131

Read Online

ACCESS | Metrics & More | Article Recommendations | Supporting Information

ABSTRACT: Scanning electrochemical microscopy (SECM) is widely used to measure local electrochemical reactivity of corroding surfaces. A major criticism of using SECM in feedback mode for corrosion studies is the requirement of an external redox mediator (RM) as it could react with the metal and affect the Nernst potential at the metal−solution interface. Consequently, it becomes challenging to differentiate the interference caused by the RM from the local reactivity of the metal. Herein, a multiscale electrochemical approach is presented to investigate the effect of RM choice on the corroding substrate. Two common RMs, ferrocenemethanol and hexaammineruthenium(III) chloride, were used to perform SECM over copper and aluminum. It was found during macroscale electrochemical measurements that $Ru(NH)_6^{3+}$ acted as an oxidant and promoted corrosion. The SECM feedback behavior varied for copper depending on the RM used, suggesting that the corrosion reactions controlled the negative feedback mechanism, not the formation of an insulating passive film. The passivated aluminum surface consistently exhibited negative feedback, regardless of the RM used. SECM approach curves also displayed a distortion in the steady state current, which was caused by the deposition of substrate-generated species on the microelectrode. These deviations in feedback response were accounted for during analysis through incorporation into a finite element model to accurately extract the RM kinetic rate constants. The importance of understanding these processes is highlighted to avoid misinterpretation of passive behavior and advances toward a more quantitative use of SECM for corrosion studies.

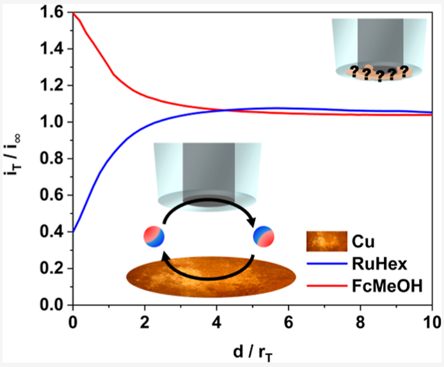

■ INTRODUCTION

Corrosion is a thermodynamically favorable process that costs society 3.4% of our global domestic products.[1] Oxidation of the world's metallic infrastructure poses an environmental threat of heavy metal contamination, jeopardizes mechanical integrity and safety of objects, and contradicts sustainability.[2] Many corrosion failure mechanisms stem from localized attack due to microstructural heterogeneities and defects, such as metallic/nonconductive inclusions,[3] grain boundaries,[4] different crystallographic orientations,[5] and dislocations, especially in halide-rich environments.[6−9] Local breakdown mechanisms are complicated by the application and residuals of stress.[10]

Scanning electrochemical microscopy (SECM) has become a vital technique in corrosion research to measure local reactivity of corroding metals and elucidate local corrosion mechanisms. The technique's high spatial resolution stems from using an ultramicroelectrode (UME). The UME can be used amperometrically or potentiometrically while scanned close to the substrate's surface to collect local current or potential maps of the metal studied. There are different operating modes of SECM that have been used to study corroding metals, including feedback mode,[11,12] generation-collection mode,[13,14] redox competition mode,[15,16] AC mode,[17,18] and potentiometric mode.[19,20] The use of SECM in corrosion science has been reviewed by many authors over the past decade.[21−25]

Feedback mode is the most popular for corrosion studies.[21] In this mode, a redox mediator (RM) is added to the electrolyte to probe the substrate's local electrochemical reactivity. The RM should be stable in solution and undergo fast heterogeneous kinetics at the UME. The regeneration of the mediator at the substrate's surface then determines the feedback current. The current is also sensitive to the distance between the UME and the substrate. Quantitative analysis of the substrate's local reactivity can be realized by performing approach curve measurements at regions of interest, typically identified by a previous current map. Typically, a negative feedback response is a verification of the presence of an insulating passive film over the corroding metal. Electroactive regions that may play a role in local breakdown tend to present positive feedback behavior. Established analytical approxima-

Received: February 3, 2024
Revised: May 9, 2024
Accepted: May 13, 2024
Published: May 22, 2024

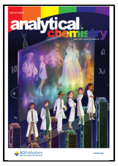

https://doi.org/10.1021/acs.analchem.4c00683

tions can be used to relate the tip-to-substrate distance and the measured current to the RM's kinetic rate constant at the substrate's surface,[26] where efforts have been made to ensure the accuracy of the fitting procedure.[27] SECM in feedback mode has been used to estimate rate constants at distinctive features,[28] detect surface heterogeneities,[29,30] and reveal passive film formation.[31,32]

Despite their popularity in corrosion science, utilizing the analytical approximations for feedback mode has some fundamental assumptions that may be compromised when studying an actively corroding substrate. For instance, the surface area of the region being probed is assumed to be infinitely larger than the UME. In reality, many microstructural features are within the same dimensions as the UME, where modeling the system's estimated geometry is required to extract local kinetic parameters.[3] In addition, when positive feedback is measured at a conductive surface, the feedback mechanism (i.e., RM regeneration) is assumed to be due to the opposite reaction occurring at a different location along the surface to liberate/consume the electron(s) needed to regenerate the mediator. If regeneration is not measured, then the substrate is considered to be insulated. Lastly, the RM is assumed to be chemically stable and unreactive toward the substrate.

Unlike inert electrodes such as Pt, C, and Au, corroding metals do not reach an equilibrium but react with their environment through dynamic electrochemical and chemical processes. The steady-state potential measured at a corroding metal's solid−liquid interface, known as the corrosion potential, is thermodynamically and kinetically determined through the mixed potential theory that outlines how the concentration of metal ions and reducing species influence potential. Thus, depending on the redox potential and charge of the mediator, it is possible that the mediator can react with the substrate and alter the corrosion potential. When employing an RM to study a corroding material using SECM, it is important to understand whether such reactions take place, as SECM feedback measurements performed over a metal at its corrosion potential (or open-circuit potential, OCP) may not reflect the true reactivity of the metal.

Although many SECM corrosion reviews raise concerns about the influence of RMs on corrosion, the number of studies investigating this is limited. Some early work performed by Basame and White showed that the choice of mediator was an important system-dependent parameter by observing the effect of different mediators on a Ta substrate.[33] It was shown by Unwin and Bard that electrochemical (oxidative) etching of active substrates was induced when mediators that undergo reduction during regeneration were used.[34−36] The corrosion behavior of the metal becomes convoluted with the RM regeneration reactions at the substrate, making it difficult to quantify local etching (corrosion) rates and reactivity.

To test the validity of using an RM in SECM measurements, macroscale electrochemical corrosion measurements can be performed, yet are negated in most SECM studies. Measurements of OCP, linear polarization resistance, and potentiodynamic polarization (PDP) can be done with and without the RM present to understand its influence on corrosion parameters such as corrosion potential (E_{corr}), polarization resistance (R_p), and corrosion current density (j_{corr}). The feedback mechanism can also be analyzed through studying different mediators using SECM approach curve measurements to indicate whether the surface is truly passivated. Herein, a multiscale methodology is presented that combines experimental and modeling approaches, which enables a holistic understanding of the effect of RMs on actively and passively corroding substrates in chloride-containing environments.

■ EXPERIMENTAL SECTION

Materials and Reagents. Wrought, phosphorus-doped, oxygen-free pure Cu was provided by Svensk Kärnbränslehantering (Solna, Sweden) and pure Al (99.99%) was obtained from GoodFellow (United Kingdom). Sodium chloride was purchased from Fisher Scientific (Ottawa, ON, Canada). Ferrocenemethanol (FcMeOH) and hexaammineruthenium(III) chloride ($[Ru(NH_3)_6]Cl_3$) were purchased from Sigma-Aldrich (Oakville, ON, Canada). All solutions were made using ultrapure water (18.2 MΩ cm).

Sample Preparation. All samples were ground and polished using a Metaserv 2000 Single Grinder Polisher and SiC paper (Buehler, Whitby, Canada) with grit sizes ranging from 400 to 4000 followed by either a 1 μm diamond polish (Cu) or 1 μm Alumina polish (Al) to obtain a mirror finish. All samples were rinsed with ultrapure water and dried with argon. SECM samples were fixed in EpoFix resin (Struers, Mississauga, Canada).

Macroscale Electrochemical Measurements. A VSP-300 potentiostat (BioLogic Science Instruments, Seyssinet-Pariset, France) and a K0235 Flat Cell (AMETEK Scientific Instruments, Berwyn, PA, USA) were used to perform open circuit potential (OCP) and PDP measurements. The experiments were conducted in a three-electrode cell arrangement under aerated conditions. The samples were connected as the working electrode, a saturated calomel electrode (SCE) was used as the reference electrode, and a platinum (Pt) mesh was the counter electrode. All electrochemical measurements were done at room temperature and inside a Faraday cage.

The OCPs of the samples exposed to a 0.6 M NaCl solution without any RMs were measured for 2 h to reach a steady state. Then, the solution was replaced with 1 mM of either FcMeOH or $Ru(NH)_6^{3+}$ in 0.6 M NaCl, and the OCP was recorded for another 1.5 h. After the OCP measurements, PDP measurements were performed using a scan rate of 10 mV min^{-1}.[37] The PDP started at −0.25 V vs OCP until a current limit of 1 mA cm^{-2} was reached. The corrosion properties, j_{corr} and E_{corr}, were systematically extracted by Tafel extrapolation, using a custom MATLAB code, where the fitting region for each branch was selected starting from 20 mV from E_{corr} for one decade of current.[38] All measurements statistics were done using the appropriately selected *t*-test at 95% confidence interval.

Cyclic voltammetry (CV) was performed on a glassy carbon (GC) electrode in 1 mM solutions of either redox mediator in 0.6 M NaCl electrolyte. CVs were conducted using a scan rate of 50 mV s^{-1} and the diffusion coefficients of each RM were calculated by using the Randles−Sevcik equation.[39]

Scanning Electrochemical Microscopy. A M470 scanning electrochemical workstation (BioLogic Science Instruments, Seyssinet-Pariset, France) was used. Pt ultramicroelectrodes (UMEs) with electroactive diameters of either 25 or 10 μm were fabricated according to a published procedure.[40] The UME tips were polished with 3, 1, and 0.3 μm polishing pads, followed by characterization via optical microscopy and CV.

The Cu and Al samples that were mounted in epoxy served as SECM substrates. The substrates were fixed in a sample

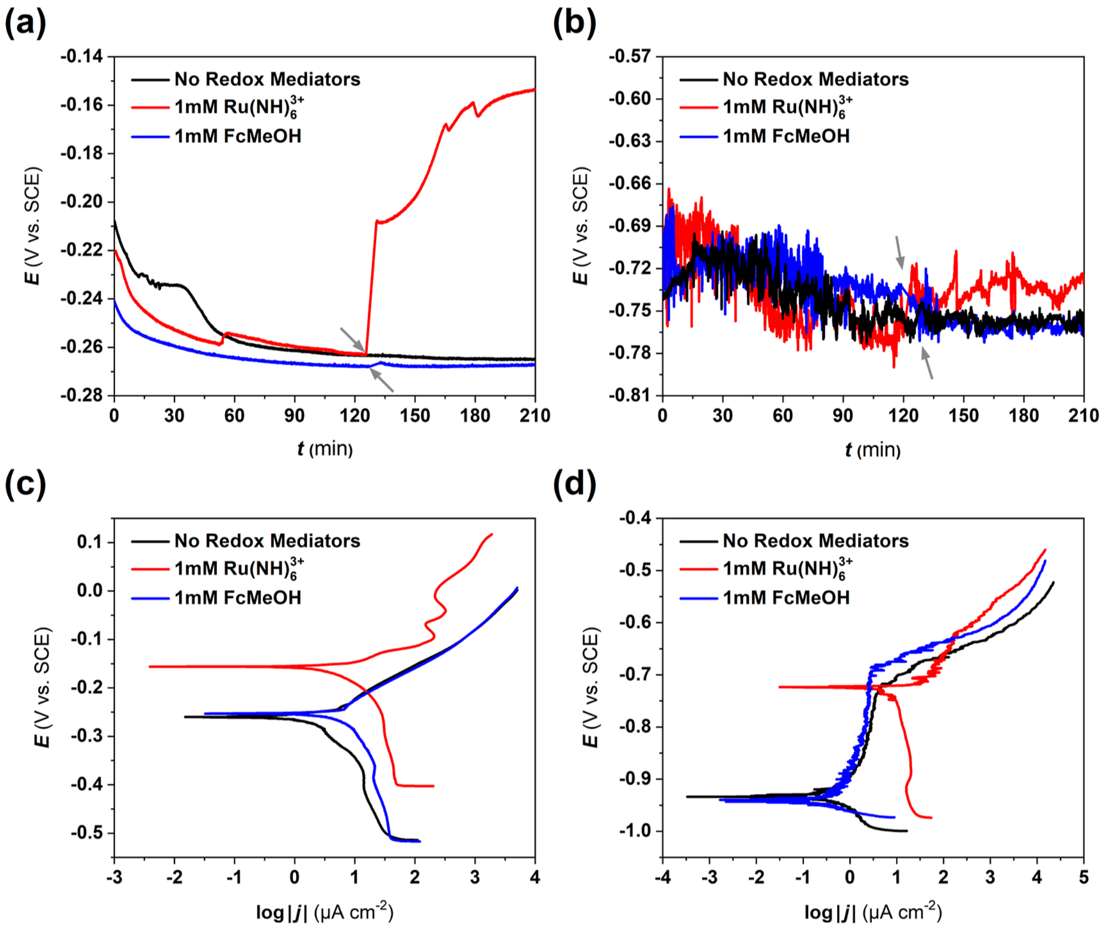

Figure 1. OCP curves of (a) Cu and (b) Al exposed to 0.6 M NaCl solution with and without the presence of the RMs. Gray arrows indicate the moment of addition of the RM in each solution upon reaching steady state. PDP curves of (c) Cu and (d) Al acquired right after OCP measurements. During PDP measurements, the initial potential was set to −250 mV vs OCP. It is noted that the apparent E_{corr} values extracted from the PDP plots for Al in 0.6 M NaCl and FcMeOH are shifted about-200 mV compared to their OCP values (Table S2). This can be attributed to the cathodic corrosion effect. When the passive film dissolves, the oxidative RM, $Ru(NH)_6^{3+}$, can then react with the underlying Al substrate and induce corrosion. The apparent E_{corr} shifted to more positive values compared to the blank sample (∼200 mV), in agreement with mixed potential theory. The apparent j_{corr} value for $Ru(NH)_6^{3+}$ was 2 orders of magnitude higher than for the other cases (Table S2), thus confirming the increase in corrosion rate of Al promoted by $Ru(NH)_6^{3+}$.

holder in such a way that the metal surface occupied approximately a quarter of the available area. The holder was leveled and fixed on an antivibration table inside a Faraday cage. Before SECM experiments, the substrates were exposed to 0.6 M NaCl, unbiased, until reaching a steady state. To perform SECM in feedback mode, the solution was exchanged for 1 mM of FcMeOH or $Ru(NH)_6^{3+}$ in 0.6 M NaCl electrolyte. CVs were recorded using a scan rate of 10 mV s^{-1} to verify UME behavior and to select the potential to apply to the UME during approach curve experiments. Approach curves were performed at 1 μm s^{-1} while holding the UME potential at 0.3 V vs SCE for FcMeOH or −0.3 V vs SCE for $Ru(NH)_6^{3+}$. An initial approach curve was obtained over the epoxy to position the UME, where it was manually stopped once a deflection in the current was observed. Once the position was established, the UME was lifted 150 μm and moved to a region over the metal to record approach curves over the metal of interest.

UME Surface Modification Experiments and Cleaning Procedure. A 25 μm Pt UME was used to conduct approach curves on Cu at OCP after the metal reached steady state in 0.6 M NaCl solution. Approach curve measurements were stopped 20 μm above the surface to prevent UME tip damage while showing changes in steady state current.

For SECM experiments performed over Cu, a cleaning procedure was required in between approach curve measurements to maintain a stable steady state current response. Chronoamperometry cycles at −0.55 V vs SCE for 5 s each were applied to the Pt UME to drive H_2 evolution on its surface. The potential of the UME was released to OCP in between cleaning cycles. Cleaning cycles were performed until the steady state current was consistent, taking approximately 8 cycles per cleaning procedure. The cleaning procedure was performed 5000 μm away from the epoxy substrate. The cleaning procedure was employed for all SECM approach curve measurements performed over Cu.

Surface Analysis. All surface morphology and chemical composition investigations of the UMEs and corroded metal substrates were analyzed by scanning electron microscopy coupled with energy-dispersive X-ray spectroscopy (SEM/EDX) using a SU3900 variable pressure SEM instrument (Hitachi, Toronto, Canada) combined with an Oxford ULTIM MAX 65 SDD X-ray detector.

The surfaces of the Cu samples post immersion in 0.6 M NaCl solutions with and without $Ru(NH)_6^{3+}$ were analyzed by X-ray photoelectron spectroscopy (XPS) using an AXIS Supra X-ray photoelectron spectrometer (Kratos Analytical, Manchester, United Kingdom). The survey scan analyses were carried out with an analysis area of 300 μm × 700 μm and a pass energy of 160 eV. The high-resolution analyses were carried out with an analysis area of 300 μm × 700 μm and a pass energy of 20 eV.

■ RESULTS AND DISCUSSION

Bulk Electrochemical Corrosion Measurements. Corrosion experiments for copper (active) and aluminum (passive) were conducted in the presence of two readily employed RMs: FcMeOH[41−47] and $Ru(NH)_6^{3+}$.[48−54] The OCP of Cu (Figure 1a) exposed to a 0.6 M NaCl solution (blank) reached an average of −268 ± 3 mV vs SCE after 2 h. Next, Cu samples were exposed to solutions containing each RM, and their OCPs were monitored for another 1.5 h to observe any changes due to polarization from the RMs present. A shift of approximately 100 mV in the positive direction was observed for the sample exposed to $Ru(NH)_6^{3+}$, with an apparent OCP of −158 ± 10 mV. Conversely, the presence of FcMeOH did not significantly alter the Cu OCP, leading to an apparent value of −266 ± 6 mV.

The OCP is a result of a mixed potential that depends on the rate of both cathodic and anodic reactions where its value lies between the reversible potentials of these reactions.[55] Because Cu's apparent OCP increased in the presence of $Ru(NH)_6^{3+}$, it is likely that $Ru(NH)_6^{3+}$ acts as an oxidant, in addition to O_2 (Figure S1), where $Ru(NH)_6^{3+}$ reduction (eq 1) induces Cu-oxidation.

$$Ru(NH)_{6(aq)}^{3+} + e^- \rightleftharpoons Ru(NH)_{6(aq)}^{2+} \tag{1}$$

The results from PDP measurements (Figure 1c) confirmed that the addition of $Ru(NH)_6^{3+}$ enhanced the corrosion rate of Cu. The apparent j_{corr} (i.e., j_{corr} measured with a RM present) was about an order of magnitude higher in the presence of $Ru(NH)_6^{3+}$ than in the other two cases (Table S2).

In contrast, FcMeOH is in its reduced state and does not act as an oxidant toward Cu. Even so, for FcMeOH oxidation to occur at the Cu surface (eq 2), a redox potential of 0.18 V vs SCE (Figure S2 and Table S1) is required, which is much more positive than the OCP of Cu. Therefore, there is no significant difference in the Cu j_{corr} values obtained with and without FcMeOH present (Table S2).

$$FcMeOH_{(aq)} \rightleftharpoons FcMeOH_{(aq)}^{+} + e^- \tag{2}$$

The E_{corr} and apparent E_{corr} values (i.e., E_{corr} measured with a RM present) extracted from PDP measurements followed a similar trend to that of the OCPs measured for Cu.

For the Al substrate, the presence of the passive oxide layer prevents surface reactions involving the RMs, so no significant shift in OCP was observed from the average value of −735 ± 7 mV vs SCE (Figure 1b). However, the passive film can break down in the presence of Cl^- ions, promoting localized corrosion. According to the experimental potential-pH diagram for Al in 3 wt % NaCl solution from Gimenez et al.,[56] at potentials between −764 and −720 mV vs SCE, the Al surface undergoes anodic pitting corrosion. This can explain the noise levels in the OCP data presented in Figure 1b.

In addition, when a negative potential is applied to Al vs its OCP, hydroxide is formed from hydrogen evolution and/or oxygen reduction, which increases the pH at the surface and solubilizes the Al oxide (eq 3).[57] This phenomenon is known as cathodic corrosion.[57−59]

$$2Al_{(s)} + 2OH_{(aq)}^- + 2H_2O_{(l)} \rightarrow 2AlO_{2(aq)}^- + 3H_{2(g)} \tag{3}$$

To confirm the experimental observations, finite element modeling (FEM) was employed to fit the PDP curves and evaluate the effect of the RM reactions on corrosion (All *R*-squared values for fitting can be found in Table S3). The model considered Cu-oxidation to Cu^{2+} ions and oxygen reduction as the main anodic and cathodic reactions, respectively. The anodic reaction involving cupric species aligned better with the model (Figure S3a) due to high polarization generating sufficient electrochemical force to drive the Cu/Cu^{2+} reaction. At OCP, cupric production is limited, resulting in the formation of only cuprous, which can react with chloride as depicted in eqs S1a and S1b.

The cathodic branch of the PDP curve in Figure S3b represents the combined effects of both oxygen reduction and the reduction of $Ru(NH)_6^{3+}$. This, in turn, leads to the anodic branch reaching higher current densities, thereby enhancing Cu-oxidation and results in an overall increase in the j_{corr}. By assuming that the oxygen reduction kinetics are constant in the presence of $Ru(NH)_6^{3+}$, any changes in the cathodic branch can be attributed to the $Ru(NH)_6^{3+}/Ru(NH)_6^{2+}$ reaction on the Cu surface. More details about the simulation can be found in the Supporting Information. The introduction of $Ru(NH)_6^{3+}$ also plays a crucial role in determining Cu's E_{corr}, which resides at a position intermediate to the three concurrent redox reactions within the system. The *R*-squared value for this fit is 0.95.

The inclusion of FcMeOH, as depicted in Figure S3c, exerts negligible influence on the polarization curve, thereby preserving the cathodic reaction in the model as exclusively oxygen reduction. This was confirmed by experimental PDP results obtained in oxygen-free conditions, where $Ru(NH)_6^{3+}$ acted as an oxidant and FcMeOH did not (Figure S4).

For Al, as illustrated in Figure S5a, the presence of a passive layer on the metal's surface is apparent. The fitted standard rate constant ($k°$) for Al-oxidation was in the range of 1.3×10^{-10} cm s^{-1}, formed on the metal surface, which hindered the oxidation of Al. However, as explained above, cathodic corrosion can destabilize this oxide barrier and then a similar trend in the PDP shifts was observed, where $Ru(NH)_6^{3+}$ promoted higher current densities (Figure S5b) whereas current densities with FcMeOH present were within the same range as the blank (Figure S5c).

UME Surface Modifications during SECM on Cu. Initial SECM approach curve measurements over Cu using a 25 μm Pt UME and FcMeOH showed a decrease in current as the number of approach curves performed increased (Figure S6a). This was attributed to UME fouling, caused by the deposition of species produced during Cu corrosion onto the UME. This inactivation of the UME surface has been observed previously in the presence of Cu and high concentrations of Cl ions by Zhao et al., where the precipitation of insoluble CuCl blocked the UME surface.[60] Similarly, the stability of the UME current was also evaluated while using $Ru(NH)_6^{3+}$. Contrary to the behavior observed when using FcMeOH, the UME current increased as the number of approach curve measurements increased (Figure S6b). The reason for such trend was attributed to an increase in surface area caused by the

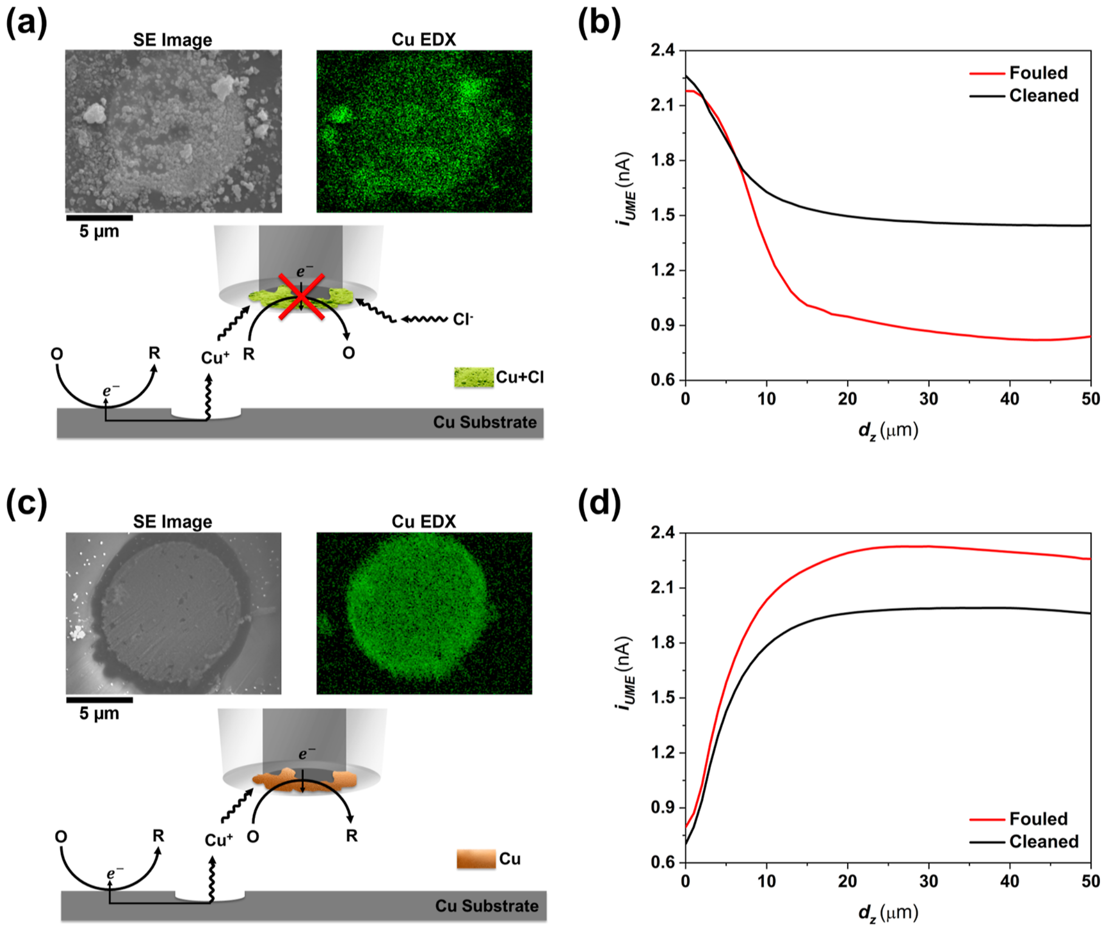

Figure 2. SEM−EDX images of the Cu distribution on the 10 μm Pt UME after performing approach curves over Cu in 0.6 M NaCl using (a) FcMeOH (oxidation at 0.3 V vs SCE) and (c) Ru(NH)$_6^{3+}$ (reduction at −0.3 V vs SCE). The complete EDX maps are available in Figure S8. Comparison of approach curves of a fouled UME and a cleaned one for the (b) FcMeOH or (d) Ru(NH)$_6^{3+}$ cases.

electrodeposition of Cu onto the UME. The onset potential for the reduction of Cu in 0.6 M NaCl is about −0.3 V vs Ag/AgCl,[61] which is close to the potential applied to the UME to induce Ru(NH)$_6^{3+}$ reduction (Figures S2 and S7b), indicating that electrodeposition of Cu onto the UME is possible.

To confirm the fouling and electrodeposition hypotheses, SEM−EDX were used to analyze the 10 μm Pt UME surfaces after the approach curves over Cu. A layer of chloride-based, and possibly some oxide-based, compounds covered the UME after SECM measurements using FcMeOH (Figures 2a and S8a). On the other hand, a Cu film was found on the UME when Ru(NH)$_6^{3+}$ was used (Figures 2c and S8b), which was confirmed by stripping voltammetry (Figure S9a). It can also be seen that the feedback response differs depending on the RM used, which is explored in the next section.

The impact of UME surface modifications during corrosion SECM experiments can influence the interpretation of the results since the current measured at the UME will be a convolution of the substrate surface kinetics and the change in UME surface reactivity and/or surface area. The supporting electrolyte choice and concentration may also play an important role in UME fouling, where the anion could induce metal complexation and/or precipitation. In this work, NaCl was used due to its popularity as a supporting electrolyte and because of its presence in groundwater where Cu containers will be placed to store used nuclear fuel.[62−64]

Although it is common to report CVs before and after SECM corrosion measurements,[3,31] inspection of the UME tip post analysis is rare. The possible necessity of an UME cleaning procedure should be checked during SECM corrosion measurements. In this work, chronoamperometry cycling (Figure S9b) was performed far from the substrate. At the selected potential of −0.55 V vs SCE, the surface of Pt promotes the hydrogen evolution reaction (HER) to mechanically remove surface deposits (Figure S10a).

This cleaning procedure successfully restored the UME steady state current to the original value obtained in bulk solution, as demonstrated by the comparison of approach curves before and after cleaning in the presence of FcMeOH (Figure 2b) and Ru(NH)$_6^{3+}$ (Figure 2d). The effectiveness of implementing the cleaning procedure in between measurements is evident in the replicate approach curves presented in Figure S10b,c for Ru(NH)$_6^{3+}$ and FcMeOH, respectively. This suggests that Cu electrodeposition is mitigated during the cleaning procedure. It should be noted that this procedure is applicable to Pt UMEs, owing to their catalytic activity toward the HER. Consequently, it may be ineffective if applied to other type of materials such as C-based UMEs.

The UME current was stable during approach curve measurements over Al. This is due to the Al passive film, which limits corrosion and UME surface modifications. Thus, the cleaning procedure was not used during SECM measurements performed over Al.

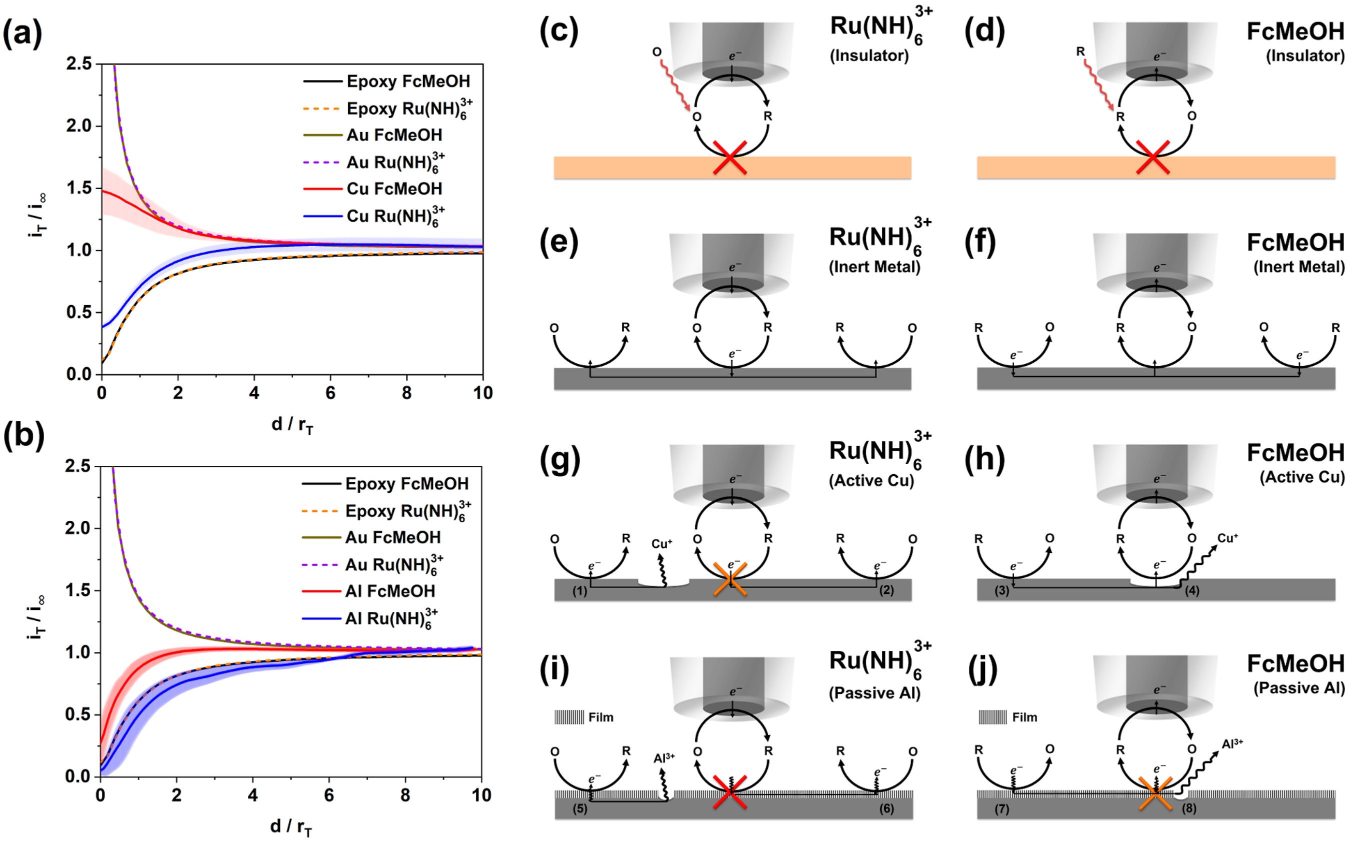

Figure 3. Normalized approach curves of (a) Cu and (b) Al exposed to 0.6 M NaCl solution with and without the presence of the RMs. Pure positive (Au) and negative (epoxy) cases are included for comparison. Schematic representation of the proposed feedback mechanisms over an insulating substrate (c,d), an inert metal (e,f), an active metal (g,h), and a passive metal (i,j). The shaded areas represent the standard deviation obtained from replicates (n = 3).

Substrate and Mediator Dependency of the Feedback Response of SECM. The feedback behavior over electrically insulating (epoxy) and inert conductive (Au) substrates was first measured using both RMs (Figure 3a,b). The approach curves performed over the epoxy portrayed negative feedback regardless of the RM used, which is governed by the hindered diffusion of the RM toward the UME, causing a decrease in the current as the tip moves closer to the insulating substrate (Figure 3c,d).

In the case of positive feedback over Au, the reduced ($Ru(NH)_6^{2+}$, Figure 3e) or oxidized ($FcMeOH^+$, Figure 3f) species generated at the UME reacted with the substrate to return to its original charged state. The mechanism for RM regeneration is mediator electrolysis supported by electron transport through the substrate,[65,66] which causes an increase in the current as the UME moves closer to the conductive surface, independent of the RM used.

For an active metal, the feedback mechanism can be influenced by corrosion. As expected, approach curves performed over Cu using FcMeOH displayed a behavior toward positive feedback. However, approach curves using $Ru(NH)_6^{3+}$ showed a negative feedback response (Figure 3a).

One hypothesis to rationalize the negative feedback observed is the formation of a passive layer when exposed to $Ru(NH)_6^{3+}$. However, results from XPS (Figure S11) and SEM (Figure S12a) demonstrated that the corrosion products on samples exposed to 0.6 M NaCl with and without $Ru(NH)_6^{3+}$ were similar, indicating that no passive film formed.

To observe positive feedback while using $Ru(NH)_6^{3+}$, the tip-generated $Ru(NH)_6{}^{2+}$ should be reoxidized at the Cu substrate to complete the feedback loop. This process requires mediator electrolysis (Process 2, Figure 3g). However, as demonstrated by the macroscale electrochemical corrosion measurements, $Ru(NH)_6^{3+}$ is an oxidant toward Cu (Process 1, Figure 3g). The consumption of $Ru(NH)_6^{3+}$ at the Cu surface created an RM depletion zone and hindered mediator electrolysis, resulting in negative feedback. As a result, the $Ru(NH)_6^{3+}$ reduction at the UME is dependent on diffusion of this species from the bulk solution.

The positive feedback behavior observed over Cu when using FcMeOH was due to successful mediator electrolysis (Process 3, Figure 3h) and the local dissolution of Cu triggered by the tip-generated oxidant species, $FcMeOH^+$ (Process 4, Figure 3h). This phenomenon has been reported,[34−36,67,68] where a flux of oxidative species restricted to a very small surface area can lead to local oxidation, or etching, of Cu.

To assess the effect of RM choice on a passive metal, approach curves were carried out over Al. Results showed that regardless of the RM employed, a negative feedback response was observed (Figure 3b). This was expected as the Al passive film is insulating; however, the magnitude the of negative feedback current was lower when $Ru(NH)_6^{3+}$ was used.

As discussed previously, the Al passive film can be attacked by Cl^- ions at defective sites to promote localized corrosion (Figure S12b). At such defective film locations, $Ru(NH)_6^{3+}$ can act as an oxidant (Process 5, Figure 3i) since the redox potential of $Ru(NH)_6^{3+}$ (−0.205 V vs SCE, Table S1) is more

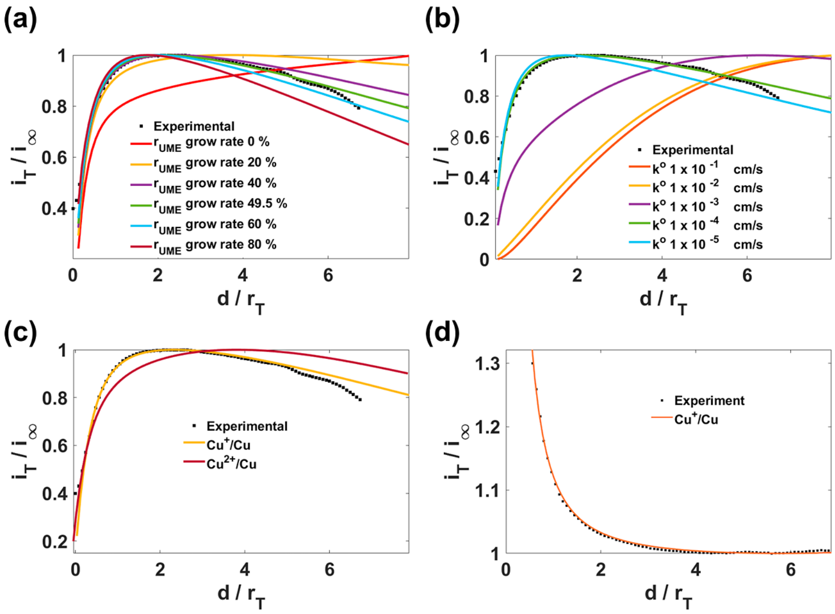

Figure 4. Comparison of experimental approach curves and simulated curves obtained using a 10 μm Pt UME over a copper substrate: (a) in the presence of $Ru(NH)_6^{3+}$ as a mediator with consideration of surface area growth, (b) variation of $Ru(NH)_6^{3+}$ rate constants on the substrate, (c) investigation of mechanistic pathways of Cu-oxidation, including the formation of cuprous (Cu^+) or cupric (Cu^{2+}) ions, and (d) utilization of FcMeOH as an RM.

positive than the OCP of Al in 0.6 M NaCl (−0.735 V vs SCE, Table S2). This is about ten times the potential difference for Al (≈500 mV) compared to Cu (≈50 mV), indicating that Al has a higher driving force for $Ru(NH)_6^{3+}$ reduction than Cu. In this case, $Ru(NH)_6^{3+}$ regeneration is limited not only by a very slow rate of electron transport through the passive film (Process 6, Figure 3i) but also by the depletion of $Ru(NH)_6^{3+}$ at the Al surface.

When using FcMeOH, the measured negative feedback current was higher (Figure 3b). Since FcMeOH does not act as an oxidant, there was no competition between the cathodic corrosion reaction and mediator electrolysis. In this case, the measured feedback current can be attributed to (1) possible mediator electrolysis occurring at the passive film (Process 7, Figure 3j), and (2) local tip-generated oxidant species, $FcMeOH^+$, that can promote localized corrosion at a defective film region (Process 8, Figure 3j). There may be other processes involved in the feedback current response, such as oxygen reduction, but those mentioned in this work appear to be the main contributors.

Without a comprehensive understanding of the mechanisms governing the feedback response that depend on the RM used, results can potentially be misleadingly attributed to passivity. For instance, $Ru(NH)_6^{3+}$ was used to study changes in passivity during applied tensile stress to a T-316 stainless steel. The RM kinetic rate constant decreased with increasing tensile load.[49] Such results were deemed counterintuitive as the applied stress would disrupt the passive film to reveal fresh (active) metal; thus, it was hypothesized that the rate constant would increase. However, the OCP of Fe is lower than Cu, indicating that the driving force for metal oxidation in the presence of the oxidant $Ru(NH)_6^{3+}$ is high. The depletion of $Ru(NH)_6^{3+}$ at the substrate during SECM approach curve measurements would result in a similar feedback response as reported here. Furthermore, when RMs that undergo reduction at the substrate were utilized in similar tensile stress SECM studies, positive feedback responses were observed.[69,70]

It is typical to fit the experimental data to analytical approximations to extract the heterogeneous rate constant of the RM at the substrate's surface. However, the approximations assume that the substrate is nonreactive, the regeneration of the RM stems from mediator electrolysis, and the electrochemical active area of the UME remains constant over time. As demonstrated, the corroding substrate can contribute to the regeneration of the RM and UME surface modifications are possible. This makes it difficult to use the analytical approximations to quantify reactivity using SECM and may lead to erroneous conclusions about the substrates local surface kinetics. To overcome this challenge, modeling is required, as described in the next section.

Modeling Electrochemical Dynamics during Approach Curves over Cu and Al Substrates. A 2D axisymmetric model was constructed for the $Ru(NH)_6^{3+}/Ru(NH)_6^{2+}$ and $FcMeOH^+/FcMeOH$ reactions on a Pt UME as it approached a Cu or Al substrate (Scheme S2). Focusing on the UME response, the model incorporated the experimentally obtained corrosion potential of the substrates. This was done to understand how the electron transfer between either $Ru(NH)_6^{3+}$ or FcMeOH occurs at the substrates during mediator regeneration. To achieve this, the concentration profiles of these species at the substrates under the corrosion potential were examined (Figure S13). This concentration profile controls the magnitude of the current that is measured by the approaching UME toward the corroding surface. Migration and convection effects were considered negligible, focusing solely on the diffusion of reactants under an applied potential. The general diffusion equation for the oxidation/reduction forms was based on Fick's diffusion law

$$\frac{\partial c_i}{\partial t} + \nabla\cdot(-D_i \nabla c_i) = J_i \qquad (4)$$

where c is the concentration, t is the time, D is the diffusion coefficient, and R is the reaction term for the species i. The values for the diffusion coefficient of both oxidized and reduced species (D) were determined experimentally (Figure S2). The concentration boundary conditions were used at outer boundaries of the phases (c_i = bulk concentration). The boundary conditions at the surface of the Pt UME and substrate were set as inward fluxes of the RMs governed by Butler−Volmer kinetics (eqs S10−S24).

For the system involving Cu as the substrate and $Ru(NH)_6^{3+}$ as the RM, a concave curvature in the experimental approach curve (Figure 4a, black dotted line) was observed. This was due to Cu deposition onto the UME during induced Cu-oxidation from the RM, resulting in a higher effective surface area. In contrast, a simulated approach curve for a constant UME surface area demonstrated a decrease in current during the approach (Figure 4a, red line).

To account for the increase in UME surface area during an approach curve measurement, systematic adjustments to UME surface area growth rates were performed to fit the experimental data. This was accomplished by continuously increasing the radius of the UME by 0.025 μm/s throughout a single approach curve. As a result, the radius of the UME extended to 7.475 μm from its initial 5 μm, representing an approximate 49.5% increase in surface area. This agreed with the experimental data of the limiting current measured in bulk solution before and after approach curves (Figure S6b).

While considering Cu deposition onto Pt, the standard heterogeneous rate constant (k°) of $Ru(NH)_6^{3+}$ on Cu was determined by varying the value from 0.1 to 1×10^{-5} cm s^{-1} and comparing the simulated approach curves to experimental data (Figure 4b). The model was in good agreement with experimental observations when k° was 1×10^{-4} cm s^{-1}.

It has been shown previously that under similar temperature and saline conditions, the predominant corrosion product of Cu are cuprous chlorides.[71−75] The model corroborates these findings as depicted in Figure 4c, where the goodness of fit between experimental approach curves is higher (R-squared = 0.94) when considering cuprous ion dissolution compared to cupric ion (R-squared = 0.92). This result is complementary to the PDP simulation results, where cupric ions gave the best fit to experimental PDP data since the substrate was externally polarized to positive potentials. This work highlights that SECM can be used to determine the oxidation state of multivalent corroding systems.

When $Ru(NH)_6^{3+}$ was replaced with FcMeOH, the model was in excellent agreement (R-squared = 0.99) with the experimental data when a k° value of 1×10^{-4} cm s^{-1} was used (Figure 4d). This result indicates that the RM regeneration surface kinetics at Cu are independent of the RM chosen and the metal's corrosion rate. The k° value suggests slow surface kinetics over Cu since it is lower than reported k° values for ferrocene derivatives on Pt.[76,77]

The simulated approach curves over Al using either $Ru(NH)_3^{3+}$ or FcMeOH are shown in Figure S14. The charge transfer coefficient (α) for both cases equal 0.10, and the k° was 1.5×10^{-6} cm s^{-1} for $Ru(NH)_3^{3+}$ and 1.5×10^{-8} cm s^{-1} for FcMeOH. The difference in values could be due to differences in RM adsorption states or that $Ru(NH)_3^{3+}$ undergoes more facile kinetics at the Al oxide interface. The extracted k° values are much lower when compared to reported values at a Pt UME surface.[77] This is due to the presence of an Al oxide film hindering the electron transfer reaction[78] and lowering the probability of electron tunneling.[79] Furthermore, the value of α in these experiments concurs with findings by Peng Sun on stainless steel (T-316).[49] α exhibits a decreasing trend as the oxide layer thickness increases. This observation implies that both kinetic parameters are influenced by the existence of a passive surface film.[49]

It is noted that the standard heterogeneous rate constants calculated from the approach curves should be considered as "apparent", owing to their dependency on the substrate kinetics, the UME surface area variation, and the reduction of mediators as part of the cathodic corrosion reaction occurring at the substrate.

■ CONCLUSIONS

This study advances the understanding of SECM in feedback mode to study corroding surfaces. The dependency of the feedback response on the RM chosen indicates that conclusions made about a metal's passivation state cannot be based solely on such experimental result.

The RM's redox potential and charge are important parameters to consider when designing an SECM corrosion experiment. Multiscale electrochemical analysis enabled the discovery that $Ru(NH)_6^{3+}$ acts as an oxidant toward the metal, causing polarization of the substrate and inducing corrosion. The consumption of $Ru(NH)_6^{3+}$ at the substrate caused a negative feedback response. The use of FcMeOH did not greatly affect macroscale corrosion properties but can induce local oxidative etching of the substrate. Moreover, the reduction of metallic ions and adherence of complexes arising from the corrosion process can cause UME surface modifications that deviate the feedback current response, where UME cleaning procedures are needed.

Although the corrosion rate of Cu increased in the presence of $Ru(NH)_6^{3+}$, the heterogeneous rate constants extracted for both RMs were the same. This highlights that the rate constants extracted over Cu depend on RM regeneration and not on the metal's corrosion rate. This is only made apparent through the comparison of the experimental and simulated data, which required the consideration of the increase in UME surface area and the corrosion mechanistic pathway.

Future work involves the exploration for an RM that does not induce oxidative etching on any length scale (i.e., is in its oxidative form and has a redox potential that is more negative than the OCP of the metal) depending on the metal of interest.

By understanding the underlying effects of the corrosion process at both the macro- and microscale, as well as on both the UME current and substrate corrosion kinetics, more accurate conclusions can be made when applying the feedback mode of SECM to study corroding metals, including metal ion oxidation states, kinetic rate constants, and rate of UME surface modifications.

■ ASSOCIATED CONTENT

Supporting Information

The Supporting Information is available free of charge at https://pubs.acs.org/doi/10.1021/acs.analchem.4c00683.

> Full experimental procedures such as materials and reagents, sample preparation, electrochemical measurements, finite element modeling details, and additional figures and tables (PDF)

AUTHOR INFORMATION

Corresponding Author

Samantha Michelle Gateman − *Department of Chemistry, The University of Western Ontario, London N6A 5B7 Ontario, Canada; Surface Science Western, The University of Western Ontario, London N6G 0J3 Ontario, Canada;* orcid.org/0000-0002-3889-9926;
Email: samantha.gateman@uwo.ca

Authors

Emmanuel Mena-Morcillo − *Department of Chemistry, The University of Western Ontario, London N6A 5B7 Ontario, Canada;* orcid.org/0000-0002-3193-0003

Ali Ebrahimzadeh Pilehrood − *Department of Chemistry, The University of Western Ontario, London N6A 5B7 Ontario, Canada*

Reza Moshrefi − *Department of Chemistry, The University of Western Ontario, London N6A 5B7 Ontario, Canada*

Ghazal Shafiee − *Department of Chemistry, The University of Western Ontario, London N6A 5B7 Ontario, Canada*

Peter George Keech − *Nuclear Waste Management Organization, Toronto M4T 2S3 Ontario, Canada*

Mehran Behazin − *Nuclear Waste Management Organization, Toronto M4T 2S3 Ontario, Canada*

Complete contact information is available at:
https://pubs.acs.org/10.1021/acs.analchem.4c00683

Author Contributions

E.M.-M. and A.E.P. contributed equally to this work. E. Mena-Morcillo and A. Ebrahimzadeh Pilehrood carried out the experiments, data analysis, and preparation of the draft manuscript. R. Moshrefi performed the simulations and data analysis. G. Shafiee completed the XPS characterization. P. Keech and M. Behazin provided project administration, scientific input, and manuscript editing. S. M. Gateman conceived the project, provided supervision and project administration, assisted with the preparation of the draft manuscript and editing, and acquired funding. All authors discussed the results and assisted during the manuscript preparation. All authors have given approval to the final version of the manuscript.

Notes

The authors declare no competing financial interest.

ACKNOWLEDGMENTS

Authors thank Dr. Jefferey Henderson, Brad Kobe, and Surface Science Western for their assistance with XPS, SEM−EDX measurements, and access to surface characterization methods as well as Prof. James Noël for using his SECM system. This work was financially supported by an NSERC Alliance grant (ALLRP 578485) and the Nuclear Waste Management Organization (NWMO).

REFERENCES

(1) NACE. *The NACE International IMPACT Study*, 2019. http://impact.nace.org/ (accessed April 28, 2019).

(2) Milošev, I.; Scully, J. R. *Corrosion* **2023**, *79* (9), 988−996.

(3) Gateman, S. M.; Stephens, L. I.; Perry, S. C.; Lacasse, R.; Schulz, R.; Mauzeroll, J. *npj Mater. Degrad.* **2018**, *2* (1), 5.

(4) Maurice, V.; Marcus, P. *Curr. Opin. Solid State Mater. Sci.* **2018**, *22* (4), 156−167.

(5) Yule, L. C.; Shkirskiy, V.; Aarons, J.; West, G.; Shollock, B. A.; Bentley, C. L.; Unwin, P. R. *Electrochim. Acta* **2020**, *332*, 135267.

(6) Macdonald, D. D. *J. Electrochem. Soc.* **1992**, *139* (12), 3434−3449.

(7) Frankel, G. S.; Sridhar, N. *Mater. Today* **2008**, *11* (10), 38−44.

(8) Soltis, J. *Corros. Sci.* **2015**, *90*, 5−22.

(9) Parangusan, H.; Bhadra, J.; Al-Thani, N. *Emergent Mater.* **2021**, *4* (5), 1187−1203.

(10) Grandy, L.; Mauzeroll, J. *Curr. Opin. Colloid Interface Sci.* **2022**, *61*, 101628.

(11) Wang, J.; Xie, L.; Han, L.; Wang, X.; Wang, J.; Zeng, H. *J. Colloid Interface Sci.* **2021**, *584*, 103−113.

(12) Qiao, Q.; Cristino, V. A. M.; Tam, L. M.; Chang, W. W.; Qian, H. C.; Zhang, D. W.; Kwok, C. T. *Surf. Coat. Technol.* **2023**, *474*, 130119.

(13) Ganborena, L.; Gonzalez-Garcia, Y.; Özkaya, B.; García, M.; García-Lecina, E.; Vega, J. M. *J. Electrochem. Soc.* **2022**, *169* (2), 021509.

(14) Lin, E.; Li, X.; Kure-Chu, S.-Z.; Li, X.; Xiao, X. *J. Mater. Eng. Perform.* **2023**.

(15) Kozlica, D. K.; Hernández-Concepción, B.; Izquierdo, J.; Souto, R. M.; Milošev, I. *Corros. Sci.* **2023**, *217*, 111114.

(16) Vega, J. M.; Ganborena, L.; Gonzalez-Garcia, Y.; Özkaya, B.; Grande, H.-J.; García-Lecina, E. *Corros. Sci.* **2023**, *210*, 110819.

(17) Pal, A.; Krishna, N. G.; Shankar, A. R.; Philip, J. *Corros. Sci.* **2023**, *221*, 111345.

(18) Cao, L.; Wang, W.; Cheng, J.; Wang, T.; Zhang, Y.; Wang, L.; Li, W.; Chen, S. *ACS Appl. Mater. Interfaces* **2023**, *15* (41), 48645−48659.

(19) da Silva, R. M. P.; Izquierdo, J.; Milagre, M. X.; Antunes, R. A.; Souto, R. M.; Costa, I. *Electrochim. Acta* **2022**, *415*, 140260.

(20) Bai, Y.-H.; Zhu, Z.-J.; Zhang, H.; Zhang, Q.-H.; Du, H.-W.; Wang, J.-Y.; Cao, F.-H. *Electrochim. Acta* **2023**, *467*, 143109.

(21) Payne, N. A.; Stephens, L. I.; Mauzeroll, J. *Corrosion* **2017**, *73* (7), 759−780.

(22) Traxler, I.; Singewald, T. D.; Schimo-Aichhorn, G.; Hild, S.; Valtiner, M. *Corros. Rev.* **2022**, *40* (6), 515−542.

(23) Jadhav, N.; Gelling, V. J. *J. Electrochem. Soc.* **2019**, *166* (11), C3461−C3476.

(24) Santana, J. J.; Izquierdo, J.; Souto, R. M. *Coatings* **2022**, *12*, 637.

(25) Skaanvik, S. A.; Gateman, S. M. *Electrochem. Sci. Adv.* **2023**, No. e2300014.

(26) Lefrou, C.; Cornut, R. *ChemPhysChem* **2010**, *11* (3), 547−556.

(27) Skaanvik, S. A.; Stephens, L. I.; Gateman, S. M.; Geissler, M.; Mauzeroll, J. *Anal. Chem.* **2022**, *94* (40), 13852−13859.

(28) Leslie, N.; Mena-Morcillo, E.; Morel, A.; Mauzeroll, J. *Anal. Chem.* **2022**, *94* (44), 15315−15323.

(29) Nowierski, C.; Noël, J. J.; Shoesmith, D. W.; Ding, Z. *Electrochem. Commun.* **2009**, *11* (6), 1234−1236.

(30) Gupta, K. K.; Yazdi, R.; Styrk-Geisler, M.; Mishin, O. V.; Ambat, R. *J. Electrochem. Soc.* **2022**, *169* (11), 111504.

(31) Gateman, S. M.; Halimi, I.; Costa Nascimento, A. R.; Lacasse, R.; Schulz, R.; Moreau, C.; Chromik, R.; Mauzeroll, J. *npj Mater. Degrad.* **2019**, *3* (1), 25.

(32) Asserghine, A.; Medvidović-Kosanović, M.; Nagy, L.; Souto, R. M.; Nagy, G. *Sens. Actuators, B* **2020**, *320*, 128339.

(33) Basame, S. B.; White, H. S. *Langmuir* **1999**, *15* (3), 819−825.

(34) Hüsser, O. E.; Craston, D. H.; Bard, A. J. *J. Electrochem. Soc.* **1989**, *136* (11), 3222−3229.

(35) Mandler, D.; Bard, A. J. *J. Electrochem. Soc.* **1989**, *136* (10), 3143−3144.

(36) Macpherson, J. V.; Slevin, C. J.; Unwin, P. R. *J. Chem. Soc. Faraday Trans.* **1996**, *92* (20), 3799−3805.

(37) ASTM International - G61-86(2018). *Standard Test Method for Conducting Cyclic Potentiodynamic Polarization Measurements for Localized Corrosion Susceptibility of Iron-, Nickel-, or Cobalt-Based Alloys*, 2018.

(38) Tait, W. S. *An Introduction to Electrochemical Corrosion Testing for Practicing Engineers and Scientists*; PairODocs Publications, 1994.

(39) Bard, A. J.; Faulkner, L. R.; White, H. S. *Electrochemical Methods: Fundamentals and Applications*; John Wiley & Sons, 2022.

(40) Danis, L.; Polcari, D.; Kwan, A.; Gateman, S. M.; Mauzeroll, J. *Anal. Chem.* **2015**, *87* (5), 2565−2569.

(41) Ye, Z.; Zhu, Z.; Zhang, Q.; Liu, X.; Zhang, J.; Cao, F. *Corros. Sci.* **2018**, *143*, 221−228.

(42) Cao, F.; Zhao, C.; You, J.; Hu, J.; Zheng, D.; Song, G.-L. *Adv. Eng. Mater.* **2019**, *21* (8), 1900363.

(43) Asserghine, A.; Medvidović-Kosanović, M.; Stanković, A.; Nagy, L.; Souto, R. M.; Nagy, G. *Sens. Actuators, B* **2020**, *321*, 128610.

(44) Varvara, S.; Caniglia, G.; Izquierdo, J.; Bostan, R.; Găină, L.; Bobis, O.; Souto, R. M. *Corros. Sci.* **2020**, *165*, 108381.

(45) He, C.; Mo, W.; Zheng, Y.; Feng, S. P.; Luo, B. *J. Alloys Compd.* **2021**, *888*, 161596.

(46) Yan, Z.-Z.; Zhang, Q.-H.; Cai, H.-R.; Li, X.-R.; Wu, L.-K.; Luo, Z.-Z.; Cao, F.-H. *Corros. Sci.* **2022**, *206*, 110541.

(47) Feng, J.; Wang, Y.; Lin, X.; Bian, M.; Wei, Y. *Surf. Coat. Technol.* **2023**, *459*, 129411.

(48) Pust, S. E.; Scharnweber, D.; Baunack, S.; Wittstock, G. *J. Electrochem. Soc.* **2007**, *154* (9), C508.

(49) Sun, P.; Liu, Z.; Yu, H.; Mirkin, M. V. *Langmuir* **2008**, *24* (18), 9941−9944.

(50) Battistel, D.; Daniele, S.; Gerbasi, R.; Baldo, M. A. *Thin Solid Films* **2010**, *518* (14), 3625−3631.

(51) Etienne, M.; Layoussifi, B.; Giornelli, T.; Jacquet, D. *Electrochem. Commun.* **2012**, *15* (1), 70−73.

(52) Etienne, M.; Dossot, M.; Grausem, J.; Herzog, G. *Anal. Chem.* **2014**, *86* (22), 11203−11210.

(53) Maho, A.; Kanoufi, F.; Combellas, C.; Delhalle, J.; Mekhalif, Z. *Electrochim. Acta* **2014**, *116*, 78−88.

(54) Xiao, C.; Elam, F.; van Vliet, S.; Bliem, R.; Lépinay, S.; Shahidzadeh, N.; Weber, B.; Franklin, S. *Carbon* **2022**, *200*, 1−9.

(55) Frankel, G. S. Fundamentals of Corrosion Kinetics. In *Active Protective Coatings: New-Generation Coatings for Metals*; Hughes, A. E., Mol, J. M. C., Zheludkevich, M. L., Buchheit, R. G., Eds.; *Springer Series in Materials Science*; Springer Netherlands: Dordrecht, 2016; pp 17−32.

(56) Gimenez, Ph.; Rameau, J. J.; Reboul, M. C. *Corrosion* **1981**, *37* (12), 673−682.

(57) Vargel, C. Chapter F.1—Protection of Aluminium. In *Corrosion of Aluminium*, 2nd ed.; Vargel, C., Ed.; Elsevier: Amsterdam, 2020; pp 383−443.

(58) Burleigh, T. D. Corrosion of Aluminum and Its Alloys. *Handbook of Aluminum*; CRC Press, 2003.

(59) Feser, R. Uniform Corrosion of Metals in Acid, Neutral and Alkaline Electrolytes. *Encyclopedia of Electrochemistry*; John Wiley & Sons, Ltd, 2007.

(60) Zhao, H.; Chang, J.; Boika, A.; Bard, A. J. *Anal. Chem.* **2013**, *85* (16), 7696−7703.

(61) Hernández-Concepción, B.; Souto, R. M.; Izquierdo, J. *Electrochim. Acta* **2024**, *474*, 143538.

(62) King, F.; Hall, D. S.; Keech, P. G. *Corros. Eng. Sci. Technol.* **2017**, *52*, 25−30.

(63) Hall, D. S.; Behazin, M.; Jeffrey Binns, W.; Keech, P. G. *Prog. Mater. Sci.* **2021**, *118*, 100766.

(64) Chen, J.; Pan, X.; Martino, T.; Lilja, C.; Behazin, M.; Binns, W. J.; Keech, P. G.; Noël, J. J.; Shoesmith, D. W. *Mater. Corros.* **2023**, *74* (11−12), 1665−1676.

(65) Bard, A. J.; Denuault, G.; Lee, C.; Mandler, D.; Wipf, D. O. *Acc. Chem. Res.* **1990**, *23* (11), 357−363.

(66) Xiong, H.; Guo, J.; Amemiya, S. *Anal. Chem.* **2007**, *79* (7), 2735−2744.

(67) Sheffer, M.; Mandler, D. *J. Electroanal. Chem.* **2008**, *622* (1), 115−120.

(68) Cornut, R.; Nunige, S.; Lefrou, C.; Kanoufi, F. *Electrochim. Acta* **2011**, *56* (28), 10701−10707.

(69) Zhu, R. K.; Luo, J. L. *Electrochem. Commun.* **2010**, *12* (12), 1752−1755.

(70) Sidane, D.; Devos, O.; Puiggali, M.; Touzet, M.; Tribollet, B.; Vivier, V. *Electrochem. Commun.* **2011**, *13* (12), 1361−1364.

(71) King, F.; Litke, C. D. *The Electrochemical Behaviour of Copper in Aerated 1 Mol·dm-3 NaCl at Room Temperature Pt 1 AECL-9571*: Canada, 1989; p 34.

(72) Tromans, D.; Sun, R. *J. Electrochem. Soc.* **1991**, *138* (11), 3235−3244.

(73) Beverskog, B.; Puigdomenech, I. *Pourbaix Diagrams for the System Copper-Chlorine at 5−100 Deg C SKI-R-98−19*: Sweden, 1998; p 56..

(74) Alfantazi, A. M.; Ahmed, T. M.; Tromans, D. *Mater. Des.* **2009**, *30* (7), 2425−2430.

(75) King, F.; Lilja, C.; Pedersen, K.; Pitkaenen, P.; Vaehaenen, M. *An Update of the State-Of-The-Art Report on the Corrosion of Copper under Expected Conditions in a Deep Geologic Repository; 1404−0344*: Sweden, 2010; p 176.

(76) Clegg, A. D.; Rees, N. V.; Klymenko, O. V.; Coles, B. A.; Compton, R. G. *J. Electroanal. Chem.* **2005**, *580* (1), 78−86.

(77) Sun, P.; Mirkin, M. V. *Anal. Chem.* **2006**, *78* (18), 6526−6534.

(78) Protsailo, L. V.; Fawcett, W. R. *Electrochim. Acta* **2000**, *45* (21), 3497−3505.

(79) Kamrunnahar, M.; Bao, J.; Macdonald, D. D. *Corros. Sci.* **2005**, *47* (12), 3111−3139.